Chemisorption on the Microsurface of Metal Clusters: Activation Barriers and Chemical Reactions for CO, N_2, O_2, and CH_4 on Al_{25}^+

Martin F. Jarrold* and J. Eric Bower

Contribution from AT&T Bell Laboratories, Murray Hill, New Jersey 07974.
Received April 11, 1988

Abstract: The chemisorption and subsequent chemical reactions of CO, N_2, O_2, and CH_4 on an Al_{25}^+ cluster have been studied over a wide range of collision energies. With CO, N_2, and CH_4 an adduct arising from chemisorption was directly observed, and activation barriers for chemisorption were deduced: 1.93 eV for CO, 3.53 eV for N_2, and 3.47 eV for CH_4. At higher collision energies chemical reactions assignable to adduct fragmentation occurred. In all cases it appears that chemisorption is dissociative (rather than molecular). With O_2 no adduct was observed (even with collision energies as low as 0.2 eV) because a very exothermic reaction follows dissociative chemisorption. An activation barrier of 0.55 eV for chemisorption of O_2 on Al_{25}^+ was deduced from the collision energy dependence of the reaction. This is slightly larger than the activation barriers found by Anderson and co-workers for Al_2^+–Al_9^+ and substantially larger than the bulk value. The size of the activation barriers observed for these different molecules with Al_{25}^+ appear qualitatively consistent with the predictions of the charge transfer model for bond activation. There is also a rough correlation between the activation barriers and the chemistry observed on aluminum surfaces.

There are several reasons for the current interest in the chemistry of metal clusters.[1-15] First, we would like to follow the development of bulk (surface) chemistry as the cluster size increases and determine how the chemistry changes as the bands develop and overlap. Second, clusters may be useful as models for surface processes. Cluster models have been employed for some time by theoreticians,[16] but until just recently they have had little hard experimental data to compare with their calculations. Third, clusters are in many respects a whole new class of chemical compound and as such they are of interest in their own right. It seems possible that metal clusters will exhibit some unique properties, unexpected from those of the atomic or bulk states.

Recently we have described a new approach to investigating chemisorption on size selected metal cluster ions.[17] A low-energy ion beam of mass selected cluster ions is passed through a gas cell. Chemisorption results in adduct formation:

$$M_n^+ + AB \rightarrow M_nAB^{+*} \quad (1)$$

and the adduct is directly monitored by mass spectrometry. The adduct is metastable since it is not stabilized by collisions and contains enough energy to dissociate back to reactants (or to other products if they are energetically accessible). However, the adduct survives long enough to be detected because the chemisorption bond energy is distributed among the large number of internal degrees of freedom in the cluster, resulting in a long lifetime toward unimolecular dissociation. By varying the collision energy between the cluster ion and the neutral species, it is possible to deduce information on the activation barrier for chemisorption and in some cases obtain an estimate of the binding energy of the adduct. Previously we applied these techniques to study the chemisorption of deuterium on bare aluminum clusters,[17] and aluminum clusters with preadsorbed oxygen,[18] as a function of cluster size for clusters with between 10 and 27 atoms.

In the work described in this paper we have taken a slightly different approach. Instead of varying the cluster size, we are varying the neutral reactant and studying, in detail, a range of reactions for one cluster size. Al_{25}^+ was selected for studying for the simple reason that it is one of the largest cluster with which we can easily perform experiments. Our previous work on the reactions of aluminum clusters with oxygen[19] and deuterium[17] suggests that for clusters with more than around 10 atoms the chemistry *generally* changes quite slowly with cluster size. For clusters with less than 10 atoms dramatic changes are observed more often. Thus we could argue that clusters with less than 10 atoms each behave like different molecules, whereas clusters with more than ten atoms behave like very small pieces of bulk. Al_{25}^+ was thus selected to be typical of this "small piece of bulk" regime. The motivation for the work described in this paper is to obtain an overview of the chemistry of the Al_{25}^+ cluster, and to compare its behavior with that of an aluminum surface and simple models for bond activation. This is the first of several papers along these lines. Future work will extend our studies of the chemistry of Al_{25}^+ and we will report analogous studies on Si_{25}^+, to compare the reactions of metal and semiconductor clusters.

Experimental Methods

The experimental apparatus and techniques have been described in detail elsewhere.[20] However, we have made several improvements over

(1) Riley, S. J.; Parks, E. K.; Nieman, G. C.; Pobo, L. G.; Wexler, S. *J. Chem. Phys.* **1984**, *80*, 1360. Richtsmeier, S. C.; Parks, E. K.; Liu, K.; Pobo, L. G.; Riley, S. J. *Ibid.* **1985**, *82*, 3659.
(2) Geusic, M. E.; Morse, M. D.; Smalley, R. E. *J. Chem. Phys.* **1985**, *82*, 590. Geusic, M. E.; Morse, M. D.; O'Brian, S. C.; Smalley, R. E. *Rev. Sci. Instrum.* **1985**, *56*, 2123.
(3) Trevor, D. J.; Whetten, R. L.; Cox, D. M.; Kaldor, A. *J. Am. Chem. Soc.* **1985**, *107*, 518. Whetten, R. L.; Cox, D. M.; Trevor, D. J.; Kaldor, A. *J. Phys. Chem.* **1985**, *89*, 567.
(4) Mandich, M. L.; Reents, W. D.; Bondybey, V. *J. Phys. Chem.* **1986**, *90*, 2315. Reents, W. D.; Mandich, M. L.; Bondybey, V. *Chem. Phys. Lett.* **1986**, *131*, 1.
(5) McElvany, S. W.; Creasy, W. R.; O'Keefe, A. *J. Chem. Phys.* **1986**, *85*, 632. McElvany, S. W.; Dunlap, B. I.; O'Keefe, A. *Ibid.* **1987**, *86*, 715.
(6) Hanley, L.; Anderson, S. L. *Chem. Phys. Lett.* **1985**, *122*, 410. Hanley, L.; Anderson, S. L. *Ibid.* **1986**, *129*, 429.
(7) Jacobson, D. B.; Freiser, B. S. *J. Am. Chem. Soc.* **1984**, *106*, 4623. Jacobson, D. B.; Freiser, B. S. *Ibid.* **1984**, *106*, 5351.
(8) Armentrout, P. B.; Loh, S. K.; Ervin, K. M. *J. Am. Chem. Soc.* **1984**, *106*, 1161. Loh, S. K.; Hales, D. A.; Armentrout, P. B. *Chem. Phys. Lett.* **1986**, *129*, 527.
(9) Freas, R. B.; Ridge, D. P. *J. Am. Chem. Soc.* **1984**, *106*, 825. Larsen, B. S.; Freas, R. B.; Ridge, D. P. *J. Phys. Chem.* **1984**, *88*, 6014.
(10) St. Pierre, R. J.; Chronister, E. L.; El-Sayed, M. A. *J. Phys. Chem.* **1987**, *91*, 5228.
(11) Knight, R. D.; Walch, R. A.; Foster, S. C.; Miller, T. A.; Mullen, S. L.; Marshall, A. G. *Chem. Phys. Lett.* **1986**, *129*, 331.
(12) Magnera, T. F.; David, D. E.; Michl, J. *J. Am. Chem. Soc.* **1987**, *109*, 936.
(13) Bohme, D. K.; Wlodek, S.; Williams, L.; Forte, L.; Fox, A. *J. Chem. Phys.* **1987**, *87*, 6934.
(14) Fayet, P.; McGlinchey, M. J.; Woste, L. H. *J. Am. Chem. Soc.* **1987**, *109*, 1733.
(15) Freas, R. B.; Campana, J. E. *J. Am. Chem. Soc.* **1985**, *107*, 6202. Freas, R. B.; Campana, J. E. *Ibid.* **1986**, *108*, 4659.
(16) See, for example: Upton, T. H.; Goddard, W. A.; Melius, C. F. *J. Vac. Sci. Technol.* **1979**, *16*, 531. Raatz, F.; Salahub, D. R. *Surf. Sci.* **1986**, *176*, 219. Pacchioni, G.; Koutecky, J. *Ibid.* **1985**, *154*, 126.
(17) Jarrold, M. F.; Bower, J. E. *J. Am. Chem. Soc.* **1988**, *110*, 70.
(18) Jarrold, M. F.; Bower, J. E. *Chem. Phys. Lett.*, in press.
(19) Jarrold, M. F.; Bower, J. E. *J. Chem. Phys.* **1987**, *87*, 5728.
(20) Jarrold, M. F.; Bower, J. E.; Kraus, J. S. *J. Chem. Phys.* **1987**, *86*, 3876.

0002-7863/88/1510-6706$01.50/0

the last few months so a fairly complete description will be given here. Clusters are generated by pulsed laser (200-Hz excimer laser operating at 308 nm) vaporization of an aluminum rod in a continuous flow of helium buffer gas. The entire source is cooled to around −135 °C in order to promote the clustering processes. Cluster ions can be derived directly from the laser plasma, or the cluster ion yield can be enhanced by firing a 1–2-kV electron beam through a small aperture into the buffer gas 0.5 cm from where the cluster ions exit the source. The electron beam enhances the cluster ion yield by around an order of magnitude, but there are concerns about whether the cluster ions are completely thermalized before they exit the source. The point of laser vaporization is 5.1 cm from the source exit, so assuming the cluster growth period is quite short (2–3 cm[21]), cluster ions coming from the laser plasma spend approximately five times longer in the buffer gas than clusters ionized by the electron beam. In the present work measurements were made mainly with cluster ions coming directly from the laser plasma. For some of the reactions reported here, measurements were also made with cluster ions generated with the electron beam. The two data sets were generally in good agreement. For the reaction between Al_{25}^+ and CH_4 a rather careful study of the effects of forming the ions by these two different means was performed. The results will be discussed below.

After exiting the source the cluster ions are gently focused into a quadrupole mass spectrometer. The ion lens in this region consists of a three-element zoom lens and horizontal and vertical deflection plates. The source is tilted 10° away from the axis of the rest of the experiment to avoid a background signal due to electronically excited neutrals from the source.[22] The voltages on the source lens system were kept low (less than 20 V) to reduce collisional activation of the clusters in the relatively high pressure of the source region. A 20-V collision of Al_{25}^+ with helium in the laboratory frame corresponds to a collision energy of only 0.12 eV in the center of mass frame. Thus while there could be a small amount of collisional activation in this region, the resulting extra internal energy will be small.

After passing through the quadrupole the size selected clusters are focused into a low-energy beam and passed through the gas cell. The ion beam focusing system in this region consists of a three-cylinder zoom lens to easily adjust the ion energy and horizontal and vertical deflection plates which are programmed to automatically adjust with the ion energy. The gas cell is at room temperature. It is 2.5 cm long and the exit aperture is 1.0 cm in diameter. The pressure in the gas cell is measured using a capacitance manometer. After passing through the gas cell, the products and unreacted ions are focused into a second quadrupole mass spectrometer where they are analyzed. At the end of this quadrupole the ions are detected by a high-voltage collision dynode and dual microchannel plates. The signals from the microchannel plates are processed using fast NIM pulse instrumentation and accumulated in an AT&T PC6300. Since the ion beam is pulsed in these experiments (pulse length around 1 ms at a repetition rate of 200 Hz), discrimination due to overlapping pulses in the detection system is a potential problem at high count rates. The data reported here were either recorded with count rates sufficiently low that there was no significant discrimination, or corrected for the discrimination.

The cross-section data reported in this paper was acquired in the "peak hopping" mode where the computer programs the quadrupole to hop along a series of peaks, counting on each peak for a preset time period. A typical experimental cycle is as follows. The ion beam energy is set and the instrument carefully refocused. A series of "peak hopping" scans are accumulated in the computer with the gas in the gas cell. The gas is then redirected using solenoid valves to flow into the vacuum chamber which houses the gas cell. Another set of "peak hopping" scans is then accumulated in the computer. This is the background set to account for reactions which occur with the background gas outside of the gas cell. The two sets are normalized, the background subtracted, and the signals converted into cross sections. The energy is then readjusted. Measurements were made every 0.1 eV, adjusting the energy down on the even points (2.6, 2.4, 2.2, etc.) and up on the odd-numbered points. In some cases there was a small (generally less than 10%) systematic difference between the scan-up and scan-down points. This is probably the result of a small drift in the pressure and was removed by running the smoothing function:

$$\sigma_i = \frac{\sigma_i + (\sigma_{i-1} + \sigma_{i+1})/2}{2} \qquad (2)$$

through the data.

The principal source of error with the type of measurements reported here is that the measured intensities of the reactant and products do not reflect their true intensities because of mass discrimination. This discrimination is expected to increase as the mass separation between reactants and products increases. In this work the reactants and products are reasonably close in mass. However, in order to estimate the uncertainties associated with these measurements some tests were performed. Mass discrimination can occur in several places: in the lens preceding the second quadrupole, in the quadrupole, and at the detector. We found that varying the voltage on the collision dynode over a wide range (±50%) had a small effect (5–10%) on the cross sections for products with a large mass difference from the reactant ion, and negligible effect for products close to the reactant ion. To minimize mass discrimination the second quadrupole was operated with a low mass resolution (generally around 5–10 amu fwhm) and a pole bias of 120–140 V. We found that small changes (generally less than 20%) could be induced in the measured cross sections by changing the voltages on the lens system preceding the second quadrupole by ±50% (enough to substantially reduce the total ion signal). From the tests described above mass discrimination does not appear to be a serious problem with these measurements. A reasonable estimate of the errors that could arise from this source is 20–40%. The larger uncertainties are expected for products that are farthest in mass from the reactant ions.

The cross sections reported in this paper were derived from the expression

$$\sigma = \ln [I_R/(I_R + \sum I_P)](1/d) \qquad (3)$$

where I_R and I_P are the reactant and product ion intensities and d is the target density, the number of reactant molecules per cm^2. The target density is estimated from the measured pressure and the gas cell length. We have not accounted for the pressure gradient caused by gas escaping from the holes in the gas cell.

Results

(A) $Al_{25}^+ + CO$. For the reaction between Al_{25}^+ and CO, two products were observed over the collision energy range studied (0.2–4.0 eV) in the center of mass): the adduct $Al_{25}CO^+$ and $Al_{23}C^+$. The neutral product associated with $Al_{23}C^+$ is probably Al_2O, which is a particularly stable molecule that is also formed as a product in the reactions of the clusters with oxygen.[19] Figure 1 shows a plot of the product ion intensities against gas cell pressure. The data shown in Figure 1 were recorded with a collision energy of 2.5 eV. At the highest pressure studied (1.0 mtorr) 10–15% of the ions are scattered out of the beam. The line and points labeled TOTAL in Figure 1 are the total product intensities ($Al_{25}CO^+$ adduct + $Al_{23}C^+$). The solid line is a linear least-squares fit to the points. The total product intensity clearly increases linearly with pressure. The intensity of the $Al_{23}C^+$ product also appears to increase close to linearly with pressure. However, the intensity of the $Al_{25}CO^+$ adduct (which is much smaller) clearly varies nonlinearly with pressure. At high pressures the intensity of the adduct levels off and stops increasing. The most likely explanation for this observation is that at the higher pressures the adduct is collisionally excited by further collisions with the reactant gas and dissociates before it can be detected. The products of this dissociation could be $Al_{23}C^+ + Al_2O$ or $Al_{25}^+ + CO$. The main product is probably $Al_{23}C^+$. Collisional activation of Al_{25}^+ before adduct formation could also occur and shorten the adduct lifetime. A rough estimate of the cross section for the collisional activation process yields a value around 90 Å^2. This is slightly smaller than the estimated hard-sphere cross section (127 Å^2[19]) suggesting that only a little extra energy is required to cause dissociation of the $Al_{25}CO^+$ adduct. Note that the estimated cross section for collisional activation is much larger than the reaction cross sections. So collisional activation is much more likely than a chemical reaction in the secondary collisions.

Figure 2 shows a plot of the cross sections for the formation of the $Al_{25}CO^+$ adduct and $Al_{23}C^+$ measured as a function of collision energy. The points are the experimental results and the lines are a nonlinear least-squares fit of a model (discussed below) to the data. The results shown in Figure 2 are the average of three independent measurements and were recorded with a gas cell pressure of 0.5 mtorr. As can be seen from Figure 2 the cross section for the adduct rises from a threshold, peaks at around 2.5 eV, and then falls with increasing collision energy. The intensity of the $Al_{23}C^+$ product rises from a threshold and increases continuously over the collision energy range studied. It appears that

(21) Riley, S. J.; Parks, E. K. In *Physics and Chemistry of Small Clusters*; Jena, P., Rao, B. K., Khanna, S. N., Eds.; Plenum: New York, 1987; p 727.
(22) Jarrold, M. F.; Bower, J. E. *J. Phys. Chem.*, submitted for publication.

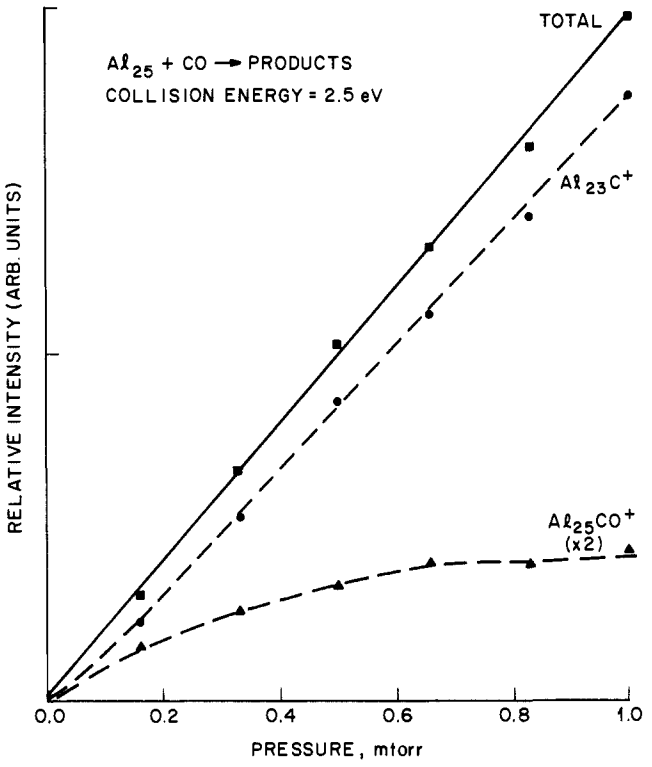

Figure 1. Plot of the relative intensities of the products against gas cell pressure for the reaction between Al_{25}^+ and CO at a collision energy of 2.5 eV. The points are the experimental results. The solid line is a linear least-squares fit to the data. The dashed lines are just guides.

the threshold for the $Al_{23}C^+$ product is shifted to slightly higher energy than the threshold for the adduct, suggesting that the $Al_{23}C^+$ product arises from dissociation of the $Al_{25}CO^+$ adduct.

(B) $Al_{25}^+ + N_2$. For the reaction between Al_{25}^+ and N_2 five products were observed: the $Al_{25}N_2^+$ adduct, Al_{24}^+, $Al_{22}N^+$, $Al_{21}N^+$, and Al_{19}^+. The gas cell pressure dependences of the intensities of these products, measured with a collision energy of 6.0 eV, are shown in Figure 3. The total product intensity increases approximately linearly with pressure. The solid line is a linear least-squares fit to the experimental data. The individual reaction products, however, all show a nonlinear pressure dependence. The intensity of the $Al_{25}N_2^+$ adduct begins to level off at the higher pressures. This is evidence for dissociation of the adduct caused by collisional activation. All the other products show a faster than linear increase with pressure. The main product from the dissociation of the $Al_{25}N_2^+$ adduct is $Al_{22}N^+$ (there could also be some Al_{25}^+ or $Al_{24}N_2^+$ which we would not be able to distinguish from the reactant Al_{25}^+ ions). The neutral product associated with $Al_{22}N^+$ is probably Al_3N. The pressure dependence of the $Al_{22}N^+$ product suggests that a small amount of this product would be formed at this collision energy without collisional activation of the adduct by secondary collisions. However, all the other products show a close to quadratic pressure dependence. The Al_{24}^+ product probably arises from collision-induced dissociation of the reactant Al_{25}^+ clusters. The other products, $Al_{21}N^+$ and Al_{19}^+, probably arise from further dissociation of the $Al_{22}N^+$ product by loss of an Al atom and a further Al_3N molecule, respectively.

Figure 4 shows a plot of the cross sections measured for the reactions between Al_{25}^+ and N_2 with a gas cell pressure of 0.5 mtorr. The experimental results shown in Figure 4 are the average of three independent measurements. The dominant product over the energy range studied is the adduct $Al_{25}N_2^+$. The cross sections for the adduct show a threshold and then rise continuously over the collision energy range studied. The threshold for the other products are shifted to higher energy than that of the adduct. The product with the lowest threshold is $Al_{22}N^+$ followed by Al_{24}^+ and the minor products, $Al_{21}N^+$ and Al_{19}^+, which apparently have close to the same threshold.

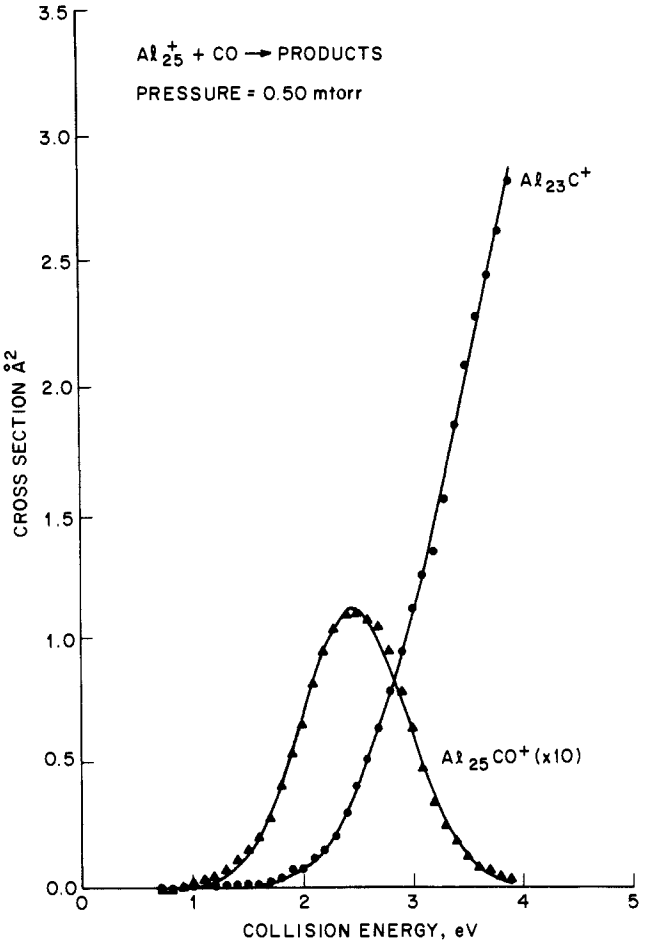

Figure 2. Plot of the cross sections for $Al_{25}CO^+$ and $Al_{23}C^+$ formation against collision energy for the reaction between Al_{25}^+ and CO. The gas cell pressure was 0.5 mtorr. The points are the experimental data and the lines are the result of a least-squares fit of a model to the experimental data (see text).

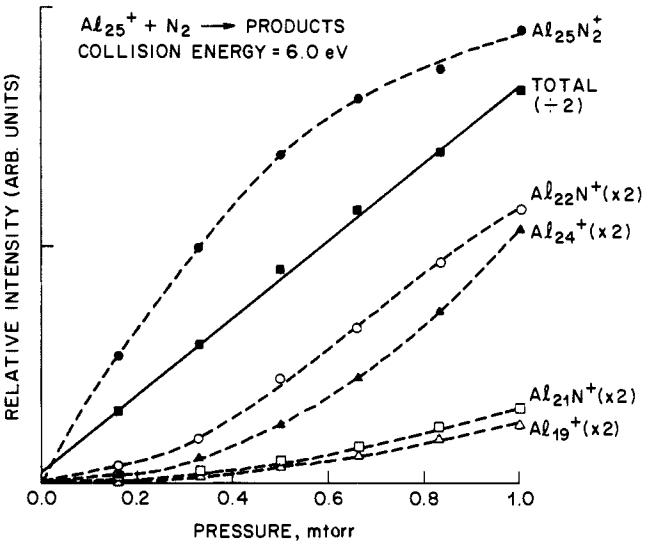

Figure 3. Plot of the relative intensities of the products against gas cell pressure for the reaction between Al_{25}^+ and N_2 at a collision energy of 6.0 eV. The points are the experimental results. The solid line is a linear least-squares fit to the data. The dashed lines are just guides.

(C) $Al_{25}^+ + O_2$. For the reaction between Al_{25}^+ and O_2 no $Al_{25}O_2^+$ adduct was observed despite a careful search down to a collision energy of 0.2 eV (in the center of mass). Consistent with our previous studies of the reactions between aluminum cluster ions and oxygen,[19] two principal reaction products were

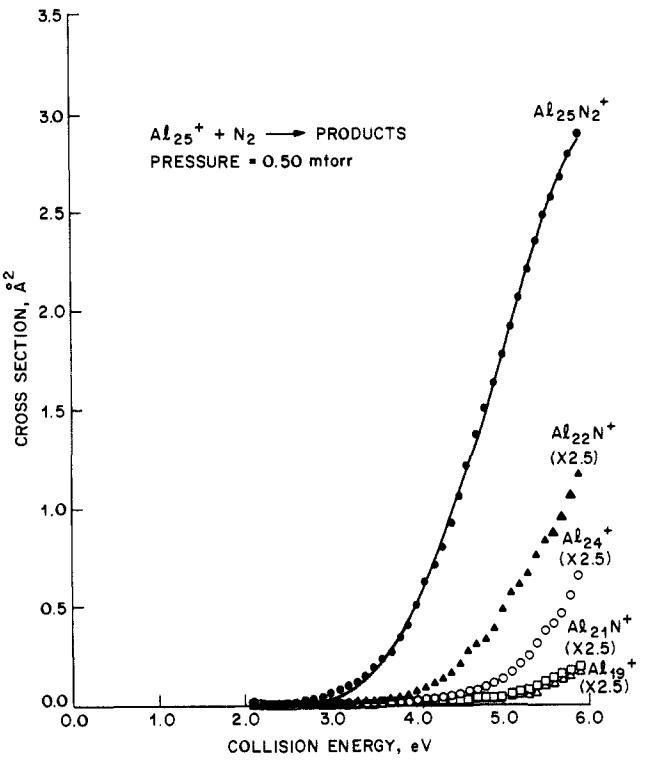

Figure 4. Plot of the cross sections for $Al_{25}N_2^+$, Al_{24}^+, $Al_{22}N^+$, $Al_{21}N^+$, and Al_{19}^+ formation against collision energy for the reaction between Al_{25}^+ and N_2. The gas cell pressure was 0.5 mtorr. The points are the experimental data and the line is the result of a least-squares fit of a model to the experimental data (see text).

observed over the collision energy range studied (0.2–4.0 eV): Al_{21}^+ and Al_{20}^+. At the higher collision energies several other minor products were observed with intensities around 1–2% of the major products. Only the major products were studied in detail. Figure 5 shows a plot of the intensities of the major products against gas cell pressure. These data were recorded at a collision energy of 4.0 eV. The pressure dependence was followed only up to 0.5 mtorr because the reaction cross sections are large (see below) and we wanted to avoid secondary reactions of the products. The solid lines in Figure 5 are linear least-square fits to the experimental data. Clearly the increase in the intensity of both products is close to linear over the pressure range studied. The significant nonzero intercept for the Al_{21}^+ product could be the result of a small depletion of this product at higher pressures by secondary reactions (to give Al_{15}^+[19]) or collision-induced dissociation of Al_{21}^+ (which is already excited by the reaction) to Al_{20}^+.

Figure 6 shows a plot of the cross sections measured for formation of Al_{21}^+ and Al_{20}^+ (with a gas cell pressure of 0.25 mtorr) against collision energy from 0.2 to 4.0 eV. Note that the cross-section scale in Figure 6 is over an order of magnitude larger than in the previous plots. This is clearly an efficient reaction. The cross sections for Al_{21}^+ increase from an apparent threshold and then begin to level off for collision energies above 1.5 eV. At higher collision energies the cross sections for Al_{21}^+ begin to fall and those for Al_{20}^+ begin to rise as sufficient energy becomes available to evaporate an aluminum atom from the Al_{21}^+ product. The cross-section data reported here are in good agreement with our previous measurements at collision energies of 1.2 and 4.2 eV.[19] We have made extensive changes to the cluster beam instrument and the way in which the cross sections are measured since the earlier work was performed. The cross sections reported here would be expected to be slightly smaller than the values we reported previously because we have accounted for several minor experimental factors which decrease the measured cross-section values slightly.

(D) $Al_{25}^+ + CH_4$. For the reaction between Al_{25}^+ and CH_4 four products were found: the $Al_{25}CH_4^+$ adduct, $Al_{24}H^+$,

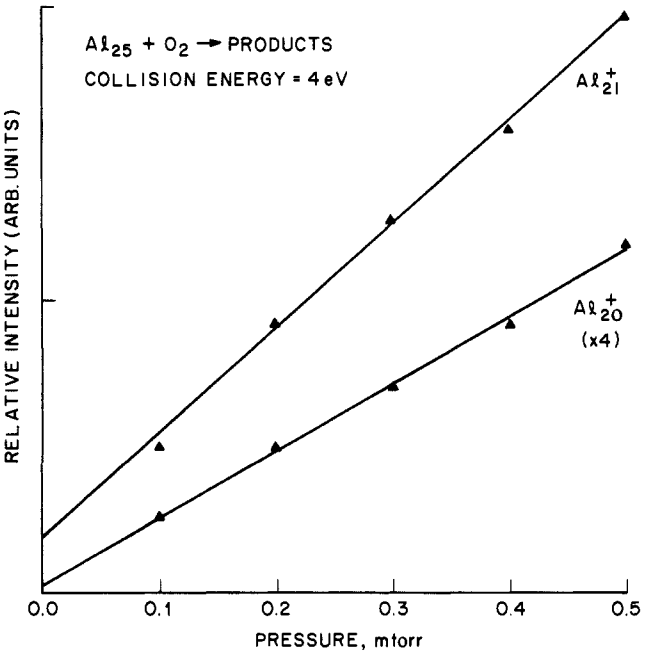

Figure 5. Plot of the relative intensities of the products against gas cell pressure for the reaction between Al_{25}^+ and O_2 at a collision energy of 4.0 eV. The points are the experimental results. The solid lines are linear least-squares fits to the data.

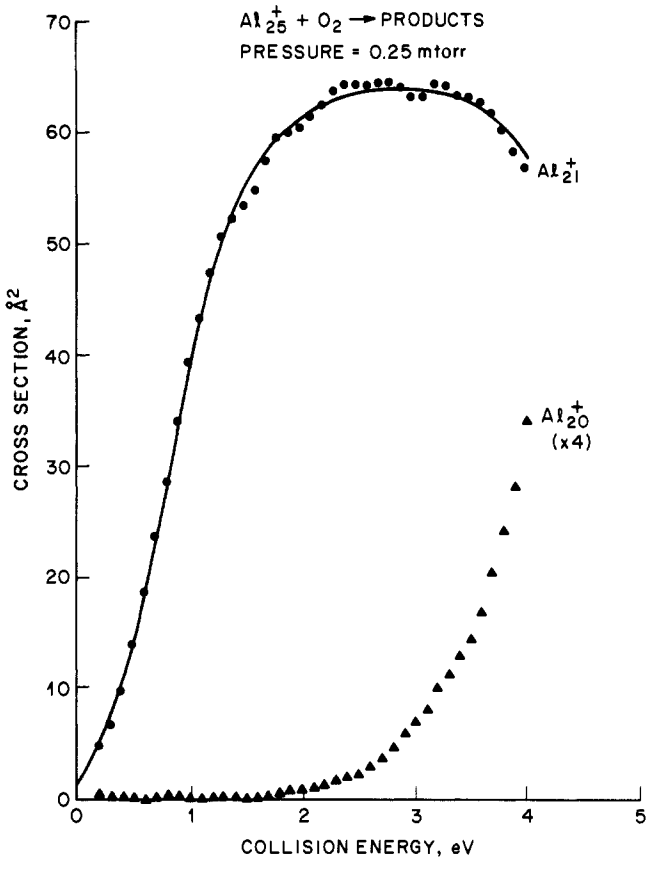

Figure 6. Plot of the cross sections for Al_{21}^+ and Al_{20}^+ formation against collision energy for the reaction between Al_{25}^+ and O_2. The gas cell pressure was 0.25 mtorr. The points are the experimental data and the line is the result of a least-squares fit of a model to the experimental data (see text).

$Al_{24}CH_3^+$, and Al_{23}^+. Because hydrogen atoms are involved in this reaction we need to consider the resolving power of the second quadrupole. The resolving power is insufficient to resolve masses separated by one mass unit when tuned up for high resolution. Thus, for example, in the case of the $Al_{24}H^+$ product, we can say

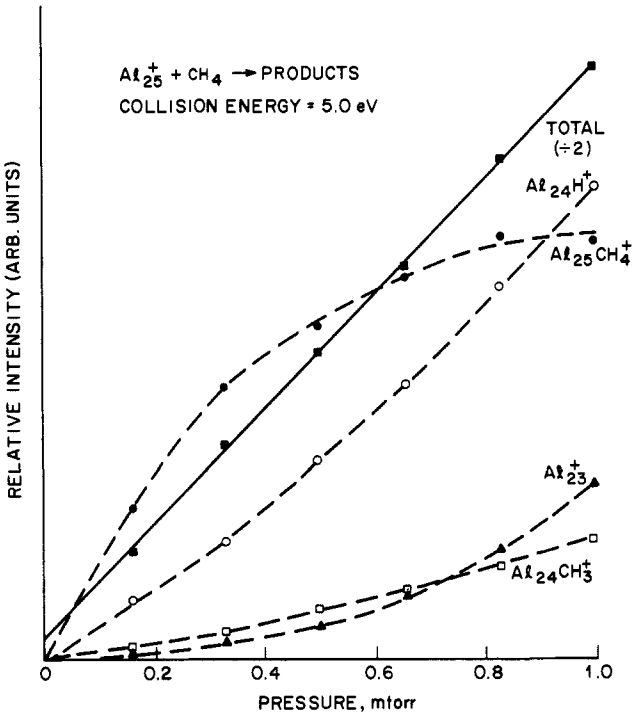

Figure 7. Plot of the relative intensities of the products against gas cell pressure for the reaction between Al_{25}^+ and CH_4 at a collision energy of 5.0 eV. The points are the experimental results. The solid line is a linear least-squares fit to the data. The dashed lines are just guides.

with confidence that the observed peak is predominantly (>80%) due to $Al_{24}H^+$, but we cannot rule out the possibility that there is a small component of Al_{24}^+ or $Al_{24}H_2^+$ present. With the low mass resolution conditions employed to make the cross-section measurements, $Al_{24}H^+$, Al_{24}^+, and $Al_{24}H_2^+$ would contribute to the $Al_{24}H^+$ signal.

Figure 7 shows a plot of the intensities of the products against gas cell pressure measured with a collision energy of 5.0 eV. The total intensity varies approximately linearly with pressure (the solid line is a linear least-squares fit to the experimental data). However, the individual products all show a nonlinear dependence on pressure. The intensity of the adduct again levels off at high pressures, indicating that collisional activation occurs, causing dissociation before the adduct is detected. The pressure dependence of the intensities of both $Al_{24}CH_3^+$ and $Al_{24}H^+$ suggests that some of these products are formed without secondary collisions, although secondary collisions enhance the amount of these products formed. The pressure dependence of the Al_{23}^+ product is close to quadratic, indicating that this product only arises from secondary collisions at the collision energy studied.

Figure 8 shows a plot of the cross sections as a function of collision energy measured with a gas cell pressure of 0.25 mtorr. The cross sections for the adduct have the lowest threshold. The cross sections for the adduct rise to a maximum at around 5.5 eV and then begin to decline. The thresholds for the other products occur in the order $Al_{24}H^+$, $Al_{24}CH_3^+$, and Al_{23}^+ at energies above the threshold for the $Al_{25}CH_4^+$ adduct. The cross sections for the $Al_{24}H^+$ product rise sharply and for collision energies above 5.7 eV exceed the cross sections for the adduct.

As mentioned above, a careful comparison between reactant Al_{25}^+ ions produced directly from the laser plasma and those generated by the electron beam was performed for the reaction between Al_{25}^+ and CH_4. The results are shown in Table I, where the ratio of the cross sections measured for the various products with the electron gun on and off are given. These data were recorded with a collision energy of 6.0 eV and a gas cell pressure of 0.5 mtorr. When the electron gun is turned on, the adduct is slightly depleted and the other products are slightly enhanced. As can be seen from Table I the differences between the cross sections recorded with the electron gun on and off are barely

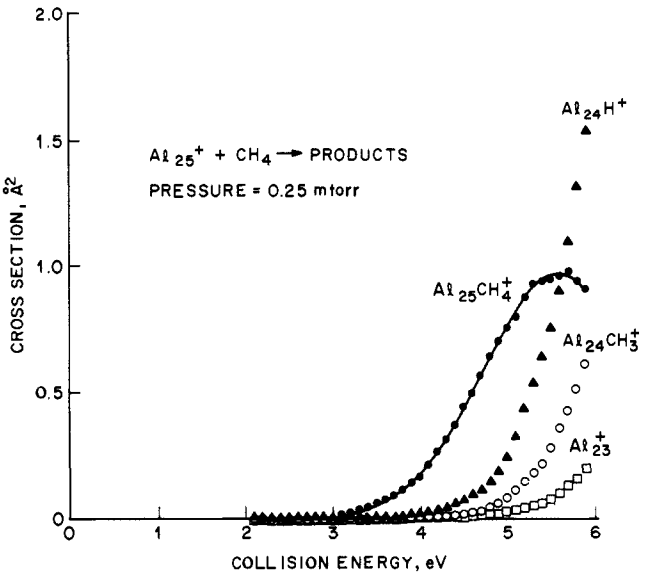

Figure 8. Plot of the cross sections for $Al_{25}CH_4^+$, $Al_{24}CH_3^+$, $Al_{24}H^+$, and Al_{23}^+ formation against collision energy for the reaction between Al_{25}^+ and CH_4. The gas cell pressure was 0.25 mtorr. The points are the experimental data and the line is the result of a least-squares fit of a model to the experimental data (see text).

Table I. Ratio of Cross Sections Measured for the $Al_{25}^+ + CH_4$ Reaction at 6.0 eV with the Electron Gun On the Off

$Al_{25}^+ + CH_4 \rightarrow$ products	
product	σ(on)/σ(off)[a]
$Al_{25}CH_4^+$	0.96 ± 0.05
$Al_{24}CH_3^+$	1.10 ± 0.09
$Al_{24}H^+$	1.01 ± 0.06
Al_{23}^+	1.10 ± 0.08

[a] Ratio of cross section measured with electron gun on and off. With the electron gun off, the Al_{25}^+ ions arise from the laser plasma. With the electron gun on, the Al_{25}^+ ions arise mainly from the electron beam.

statistically significant. However, the changes are in the direction we would expect if the ions formed by the electron beam contained slightly more energy. So these results suggest that the ions generated by the electron gun may not be completely cooled before they exit the source, but they certainly do not contain a substantial amount of excess internal energy.

Analysis of Threshold Data

The threshold for adduct formation can be related to the activation barrier for chemisorption. The threshold region is broadened, however, by the thermal motion of the target gas and the energy spread of the ion beam. To derive an accurate value for the threshold the usual approach in beam studies of this type is to simulate the experimental data with an assumed cross-section function convoluted with functions to account for the threshold broadening.[23-25] To determine the thresholds for adduct formation we used a cross-section function of the form:

$$\sigma(E) = A(E - E_0)^n \exp[-k(E - E_0,E_x,m)t] \qquad (4)$$

which we have discussed in detail elsewhere.[17] The threshold E_0, A, n, and m are adjustable parameters. $k(E - E_0,E_x,m)$ is the rate of unimolecular dissociation of the adduct (derived from RRKM theory[17]), and t is the flight time. The adduct could dissociate either back to reactants or to other products if they are energetically accessible. E_x is the energy difference between the activation barrier for chemisorption and the threshold for the

(23) Chantry, P. J. *J. Chem. Phys.* **1971**, *55*, 2746.
(24) Liftshitz, C.; Wu, R. L. C.; Tiernan, T. O.; Terwilliger, D. T. *J. Chem. Phys.* **1978**, *68*, 247.
(25) Armentrout, P. B.; Beauchamp, J. L. *J. Chem. Phys.* **1981**, *74*, 2819. Ervin, K. M.; Armentrout, P. B. *Ibid.* **1985**, *83*, 166. Hanley, L.; Ruatta, S. A.; Anderson, S. A. *Ibid.* **1987**, *87*, 2670.

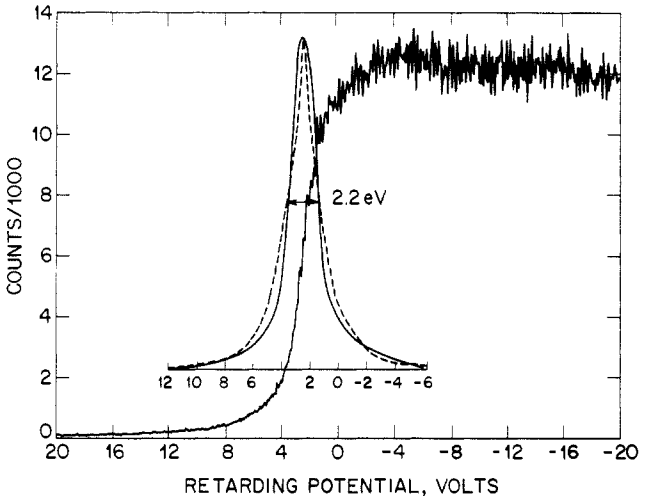

Figure 9. Energy distribution of Al_{25}^+ determined using a retarding potential analyzer. The figure shows the raw data from a scan of the energy analyzer and also the ion energy distribution determined from the experimental data by numerical differentiation. The dashed line gives the exponential ion beam energy distribution used in the simulation of the experimental data to determine the true thresholds (see text).

formation of other products. For the reaction with CO, E_x was treated as an adjustable parameter; for the other reactions, it was set at zero. For the reaction with oxygen where no adduct was observed, the reaction cross sections were simulated with the cross-section function:

$$\sigma(E) = A(E - E_0)^n/E^k \quad (5)$$

where E_0, A, n, and k are adjustable parameters.

In our previous work on the chemisorption of deuterium on aluminum clusters, the large mass difference between the reactants meant that the energy spread of the ion beam (in the center of mass frame) was essentially negligible.[17,18] With the reactions studied here the mass of the neutral reagent is larger, so we need to consider the energy distribution in more detail. Figure 9 shows a plot of the energy distribution of the ion beam measured with a retarding potential energy analyzer situated just before the second quadrupole. The figure shows the raw data from a scan of the energy analyzer and also the ion energy distribution derived from the experimental data by numerical differentiation. Typically the distribution is 2.2 eV wide (fwhm). The resolution of a retarding potential energy analyzer is determined by field penetration through the grids. Under the operating conditions employed to measure the distribution shown in Figure 9, the resolution is estimated to be 0.6 eV.[26,27] As can be seen from Figure 9 there is a significant high-energy tail on the energy distribution which cannot be accounted for by energy analyzer resolution. There is also a low-energy tail, but this could be an artifact caused by poor transmission through the energy analyzer. For a fully relaxed supersonic expansion with no slippage, the Al_{25}^+ cluster would achieve a terminal energy of 5.0 eV[28] (for a source temperature of 135 K). It is apparent from Figure 9 that the average energy is significantly lower.[29] This is not surprising since the expansion is quite mild (the backing pressure is around 20 torr at room temperature). It seems likely that the rather broad ion energy distribution we observe is due at least in part to the mild expansion (i.e., acceleration to the terminal helium velocity has started but is incomplete). It is also possible that some of the high-energy tail is due to energy picked up by the ions in the rf fields of the first quadrupole.[30]

Because of the large mass of the cluster ion the energy spread of the ion beam is still small when transferred to the center of mass frame (around 88 meV fwhm). However, the high-energy tail extends to quite large energies, and in order to account for this in the simulation of the experimental data to determine the true thresholds, the ion beam energy distribution was modeled using an exponential function of the form

$$P(E_b) = (S/2)\exp(-[(E - E_b)^2S^2]^{1/2}) \quad (6)$$

where S is a constant with a value of 0.63 for a distribution with a width of 2.2 eV (fwhm). This function is shown as the dashed line in Figure 9. The thermal motion of the target gas was accounted for using the method of Chantry.[23]

The cross-section function (eq 4 or 5) was convoluted with the functions discussed above to account for the threshold broadening. This simulation was then fit to the experimental data using a nonlinear least-squares procedure to optimize the values of the threshold and the other adjustable parameters. The solid lines shown in Figures 2, 4, 6, and 8 are the fits of the simulations to the experimental data. The values of the thresholds and the other adjustable parameters used to fit the data are shown in Table II.

Table II. Thresholds and Model Parameters Deduced from the Simulation of the Experimental Data

reaction	E_0	A	n	m	E_x	k
$Al_{25}^+ + CO$	1.93 ± 0.30	0.86	1.65	2.43	2.08	
$Al_{25}^+ + N_2$	3.53 ± 0.30	0.96	1.37	2.05	0.0[a]	
$Al_{25}^+ + O_2$[b]	0.55 ± 0.30	95.7	1.04			1.19
$Al_{25}^+ + CH_4$	3.47 ± 0.30	0.32	1.78	2.46	0.0[a]	

[a] Assumed to be 0.0. [b] No adduct was observed so the total reaction cross section was modeled.

Discussion

(A) $Al_{25}^+ + CO$. The experimental data for this reaction suggest a mechanism in which the CO dissociatively chemisorbs on the cluster and then an Al_2O molecule is desorbed leaving an $Al_{23}C^+$ product. From the wide range of studies of CO chemisorption on metal surfaces that have been performed,[31] we would anticipate that CO might chemisorb either dissociatively or intact on the cluster. The observation of $Al_{23}C^+$ products suggests (but is not proof) that chemisorption is dissociative to yield separated O and C atoms. The activation barrier of 1.93 eV deduced from the threshold for adduct formation is therefore likely to be associated with the cleavage of the strong CO bond (D(C–O) = 11.11 eV[32]).

The large $Al_{23}C^+$ signal and small $Al_{25}CO^+$ adduct signal, and the shape of the cross-section data shown in Figure 2, suggest that the threshold for loss of an Al_2O molecule from the adduct lies below the activation barrier for CO chemisorption as shown schematically in Figure 10a. The simulation of the cross-section data (solid lines in Figure 2) was based on this assumption. We first fit the total reaction cross section ($Al_{25}CO^+$ adduct + $Al_{23}C^+$) using a cross-section function of the form

$$\sigma(E) = A(E - E_0)^n \quad (7)$$

adjusting A, E_0, and n in the least-squares analysis. We then took the values of these parameters and fit the cross-section data for the $Al_{25}CO^+$ adduct only adjusting the parameters associated with the dissociation of the adduct to $Al_{23}C^+$. As can be seen this

(26) An estimate of the resolution can be obtained from $\Delta E = 2sV/\pi d$, in which s is the spacing between the grid wires, d is the separation between the plates, and V is the voltage on the electrodes on either side of the one carrying the retarding potential. This can be simply derived from considering the voltage in the center of a circular aperture inserted between two electrodes at the same potential.[27]

(27) Jacob, L. *An Introduction to Electron Optics*; Methuen: London, 1951.

(28) Levy, D. H.; Wharton, L.; Smalley, R. E. In *Chemical and Biochemical Applications of Lasers*; Moore, C. B., Ed.; Academic: New York, 1977. Anderson, J. B. In *Molecular Beams and Low Density Gas Dynamics*; Wegner, P., Ed.; Marcel Dekker: New York, 1974.

(29) In an earlier study we reported that the ions apparently attained a kinetic energy close to the value expected for a fully relaxed expansion.[20] The energy analyzer was operated with much lower resolution in that work. We now recognize that this will cause a shift in the measured average energy to higher values. This probably accounts for the discrepancy.

(30) Evans, B. E.; Supple, R. W. *J. Vac. Sci. Technol.* **1971**, *8*, 270.

(31) See, for example: Steinruck, H. P.; D'Evelyn, M. P.; Madix, R. J. *Surf. Sci.* **1986**, *172*, L561. Dumas, P.; Tobin, R. G.; Richards, P. L. *Ibid.* **1986**, *171*, 555. Broden, G.; Rhodin, T. N.; Brucker, C.; Benbow, R.; Hurych, Z. *Ibid.* **1976**, *59*, 593.

(32) All thermochemical information derived from: Rosenstock, H. M.; Draxl, K.; Steiner, B. W.; Herron, J. T. *J. Phys. Chem. Ref. Data* **1977**, *6*, Suppl. No. 1.

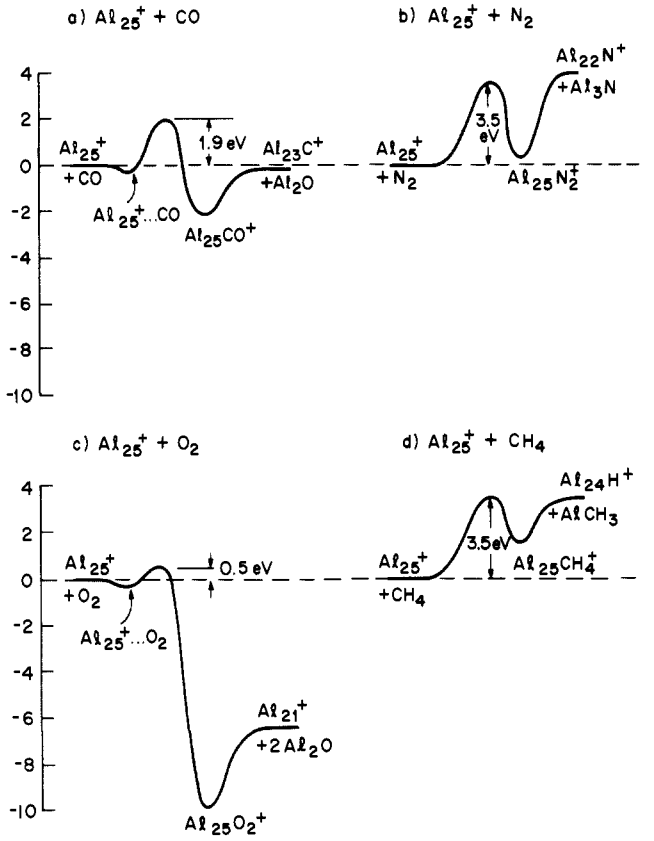

Figure 10. Qualitative potential energy curves for the reactions between (a) Al_{25}^+ and CO, (b) Al_{25}^+ and N_2, (c) Al_{25}^+ and O_2, and (d) Al_{25}^+ and CH_4. The activation barriers are from the measurements reported in this paper. The desorption energies are only crude estimates.[47]

provides an excellent overall fit to the experimental data and supports the mechanism discussed above. The best fit to the experimental data was found with the threshold for loss of Al_2O 2.1 eV below the activation barrier for chemisorption of CO. The absolute value of this quantity is probably not very reliable, but it supports the qualitative conclusions made above.

(B) $Al_{25}^+ + N_2$. Dissociative and nondissociative chemisorption of N_2 has been observed on metal surfaces.[33] However, compared to CO, chemisorption of molecular N_2 is less common and the heats of nondissociative chemisorption are generally lower. As can be seen from Table II the activation barrier measured for chemisorption of N_2 onto Al_{25}^+ is 3.53 eV. This is close to twice the activation barrier observed with CO (which is isoelectronic with N_2), even though the dissociation energy of N_2 ($D(N_2)$ = 9.76 eV) is actually slightly smaller than the dissociation energy of CO. The observation of products arising from cleavage of the N_2 bond ($Al_{22}N^+ + Al_3N$) suggests that chemisorption of N_2 on Al_{25}^+ is dissociative. However, the intensity of these products is small and their threshold shifted considerably above the threshold for the adduct (even at 6 eV it appears that a substantial fraction of the observed $Al_{22}N^+$ product results from collisional activation in secondary collisions), so this evidence for dissociative chemisorption is considerably less convincing than in the case of CO on Al_{25}^+. It is apparent from Figure 4 that the $Al_{25}N_2^+$ adduct is observable over a wide range of collision energies unlike the $Al_{25}CO^+$ adduct which rapidly dissociates at the higher collision energies. This suggests that the $Al_{25}N_2^+$ adduct is quite strongly bound and that the thresholds for the other products are not substantially below the activation barrier for N_2 chemisorption. These ideas about the $Al_{25}N_2^+$ potential energy surface are illustrated schematically in Figure 10b.

From Figure 4 it can be seen that there is excellent agreement between the experimental data and the simulation using the assumed cross-section function. However, the agreement is not perfect. There is a minor discrepancy in the fit around a collision energy of 3 eV. The discrepancy is small and we would not mention it further, but it raises a general point about these measurements. We have assumed that there is only one activation barrier in our model. It is not difficult to imagine that there could be several different chemisorption sites on Al_{25}^+ each with slightly different activation barriers (or there could be several structural isomers of Al_{25}^+), in which case the threshold we would determine would be an average (weighted by the number of different sites). So a possible explaination for the type of discrepancy seen in Figure 4 is that it is due to chemisorption at a different type of site with a slightly lower activation barrier. Since the discrepancy is small in this case it could also be due to minor inaccuracies in the experimental data or approximations and assumptions made in the simulation.

The neutral product associated with $Al_{22}N^+$ is not directly observed but is probably Al_3N. This is a rather unusual molecule. However, in view of the other neutral products that we have found in different reactions (AlD[17] and Al_2O[19]), it is quite obvious that the aluminum atom is preferring to keep its 3s subshell intact and only use its 3p electron to form chemical bonds. Hence the neutral product is Al_3N not AlN. Bulk aluminum nitride (AlN) is a hard, stable material with a close structural relationship to diamond. Presumably much of its stability comes from the formation of an extended lattice.

(C) $Al_{25}^+ + O_2$. Al_{25}^+ undergoes an efficient chemical reaction with O_2, and no $Al_{25}O_2^+$ adduct was observed even at collision energies as low as 0.2 eV. Measurements were not performed below 0.2 eV for the following reason. As the ion energy is lowered the beam current stays reasonably constant down to a collision energy of 0.5 eV. Then the intensity starts to drop and the drop becomes more rapid as the energy is lowered further. At a collision energy of 0.2 eV the intensity has dropped to around a third of its high-energy value, and the energy distribution has begun to be distorted by the lower transmission of the lower energy ions in the distribution.

Previously we have shown that it is possible to generate aluminum cluster oxide species such as $Al_{25}O_2^+$ by adding a trace of oxygen to the buffer gas in the source.[34] So $Al_{25}O_2^+$ is a stable species. However, the failure to observe adduct formation in the reaction is not too surprising. As we have discussed elsewhere,[19] the reaction between aluminum clusters and oxygen:

$$Al_{25}^+ + O_2 \rightarrow Al_{21}^+ + 2Al_2O \qquad (8)$$

is exothermic by around 7.5 eV. It appears from the data shown in Figure 6 that there could be a small threshold associated with the reaction. To deduce an accurate value for this threshold, the data were simulated using the cross-section function given in eq 5. As can be seen from Figure 6 the simulation is an excellent fit to the experimental data (in fact, the total cross-section data were simulated and the line shown in Figure 6 is the simulated total cross section minus the experimental cross sections for Al_{20}^+). The threshold deduced from this analysis is 0.55 eV. In view of the large exothermicity of the overall reaction (around 7.5 eV), the observation of such a threshold is somewhat surprising. Since the reaction is so exothermic the threshold can only reasonably be due to an activation barrier in the entrance channel; i.e., it must be associated with the chemisorption of the oxygen onto the cluster before the resulting $Al_{25}O_2^+$ adduct rapidly dissociates to give the Al_{21}^+ product. A schematic potential energy diagram for the $Al_{25}^+ + O_2$ system illustrating this is shown in Figure 10c.

Anderson and co-workers[35] have recently reported measurements of the thresholds for the reactions of aluminum clusters (with two to eight atoms) with oxygen. The general shape of the

(33) See, for example, Miki, H.; Kato, K.; Kawana, A.; Kioka, T.; Sugai, S.; Kawasaki, K. *Surf. Sci.* **1985**, *161*, 446. Whitman, L. J.; Bartosch, C. E.; Ho, W.; Strasser, G.; Grunze, M. *Phys. Rev. Lett.* **1986**, *56*, 1984. Breitschafter, M. J.; Umbach, E.; Menzel, D. *Surf. Sci.* **1986**, *178*, 725. Kuwahara, Y.; Jo, M.; Tsuda, H.; Nishijima, M. *Ibid.* **1987**, *180*, 421.

(34) Jarrold, M. F.; Bower, J. E. *J. Chem. Phys.* **1987**, *87*, 1610.

(35) Ruatta, S. A.; Hanley, L.; Anderson, S. L. *Chem. Phys. Lett.* **1987**, *137*, 5.

cross sections versus collision energy plots they measured are strikingly similar to the one reported here for Al_{25}^+. One major difference is, however, that the cross sections for Al_{25}^+ are around five times larger than those for the smaller clusters. They found barriers which increased from 0.09 eV for the trimer up to 0.25 eV for Al_7^+, and then dropped slightly to 0.22 eV for Al_8^+. Recently, Ruatta and Anderson have extended these measurements up to Al_9[36] and found that the activation barriers apparently continue to drop slightly with increasing cluster size. Since oxygen readily chemisorbs on aluminum surfaces[37] where there certainly cannot be a substantial activation barrier, one would expect the activation barrier to continue to drop with increasing cluster size. From the threshold of 0.55 ± 0.3 eV deduced from our data on Al_{25}^+, this apparently does not happen. It would be interesting to extend these measurements to clusters with between 9 and 25 atoms. However, the implication of our results is clear: whatever it takes to make these clusters behave like the bulk has not happened with a 25-atom cluster.

(D) $Al_{25}^+ + CH_4$. Methane chemisorbs on Al_{25}^+ and the resulting $Al_{25}CH_4^+$ adduct is directly observable. From a simulation of the cross sections for adduct formation, we deduced an activation barrier of 3.47 eV for chemisorption of CH_4 on Al_{25}^+. As can be seen from Figure 8 there is excellent agreement between the simulation and the experimental results. At collision energies above the threshold for adduct formation, $Al_{24}H^+$ and $Al_{24}CH_3^+$ are observed as products. The neutral products associated with these ions are probably $AlCH_3$ and AlH, respectively. These products are consistent with the idea that the aluminum atom likes to keep its 3s subshell intact. The most reasonable structure for methane dissociatively chemisorbed on an aluminum cluster is a separate H and CH_3 group bound to the surface. Such a structure is clearly consistent with the observed reaction products. A schematic potential energy surface for the $Al_{25}^+ + CH_4$ system is shown in Figure 10 where it can be compared with those for the other systems studied.

The activation of C–H bonds is an important process. With an activation barrier for chemisorbing CH_4 of 3.47 eV, it appears that Al_{25}^+ does a remarkably poor job. In fact, from the CH_3–H bond energy (4.44 eV)[32] and the measured activation barrier, it appears that it is necessary to supply almost enough energy to break a CH_3–H bond before it will chemisorb on an Al_{25}^+ cluster. It is particularly instructive to compare the activation barrier found for CH_4 chemisorption with that found in our previous work for the chemisorption of D_2 on Al_{25}^+ (1.99 eV).[17] The CH_3–H bond energy (4.44 eV) is remarkably close to the H–H bond energy (4.48 eV). Yet the activation barrier for chemisorption of CH_4 on Al_{25}^+ is almost twice the activation barrier for chemisorbing D_2. A possible contributing reason for this large difference is steric effects.[38]

(E) Comparison with Chemistry of Neutral Clusters. Cox and co-workers have recently performed a study of the chemistry of neutral aluminum clusters using the fast flow reactor technique.[39] This technique probes chemisorption reactions at close to thermal energies (300–500 K). They investigated the reactions of H_2, H_2O, O_2, CH_3OH, CH_4, and CO. With CH_4 they found no evidence for reaction with any cluster size. This is consistent with our measurement of a large activation barrier for chemisorption on Al_{25}^+. With CO they did not directly observe any products. However, they found a small amount of depletion of the reactant cluster for Al_6 when the CO was added to the flow tube. So Al_6 probably does react with CO, and the larger clusters may react, but more slowly. As we discuss in more detail below these results are not inconsistent with our measurements.

The comparison with the O_2 reactions is perhaps the most fascinating. In the studies of the neutral reactions Al_nO_2 products were directly observed. The reactivity was found to fall rapidly on going from the dimer to the trimer and then steadily increase, reaching the dimer level at around Al_{30}. In our previous work on the reactions of aluminum cluster ions with oxygen,[19] we argued that the Al_nO_2 products observed by Cox and co-workers could not correspond to dissociative chemisorption, since even in the high pressure of a flow tube reactor the energy released in forming the Al–O bonds would rapidly fragment the adduct before it could be collisionally stabilized (the energetics of the reactions of neutral and positively charged aluminum clusters with oxygen are expected to be quite similar). The activation barrier of 0.55 eV found in this work for the reaction of Al_{25}^+ with O_2 lends some additional support to these ideas. The scheme we propose is illustrated in Figure 10c. The O_2 and aluminum cluster can form a weakly bound adduct. The weakly bound adduct dissociates too rapidly to be directly observed in our experiments, but with collisional stabilization it can be directly observed in the flow tube experiments. In the flow tube studies there is insufficient energy to overcome the activation barrier. As we raise the kinetic energy in our experiments we can overcome the barrier associated with cleavage of the O_2 bond, dissociative chemisorption occurs, and the energy released results in rapid fragmentation of the adduct to yield $Al_{21}^+ + 2Al_2O$.

(F) Comparison with Surface Chemistry of Bulk Aluminum. An obvious question we are concerned with in performing these studies is the relationship between the chemistry we observe with Al_{25}^+ to that found with bulk aluminum. Ultimately we hope to understand any observed differences in terms of the electronic properties of the cluster, with particular reference to the development of bulk metallic properties. With aluminum clusters, for example, the development and overlap of the 3s and 3p bands is likely to be an important factor. One rather obvious way in which our Al_{25}^+ cluster differs from the bulk is that nearly all the atoms in the cluster are surface atoms. From the structureless packing model of Riley and co-workers,[40] only two to three of the atoms in Al_{25}^+ are bulk atoms.

CO has been found to undergo weak molecular chemisorption on an Al(100) surface.[41] The CO was found to desorb at a temperature of 125 K from which an adsorption energy of 0.35 eV was deduced. There have been several theoretical calculations for the chemisorption of CO on aluminum using cluster models.[42,43] The calculations are in reasonable agreement; molecular CO is weakly bound to the surface and the bonding is due mainly to charge donation from the metal to the CO $2\pi^*$ orbital. Unfortunately, dissociative chemisorption was not considered in these theoretical studies. It seems likely that the weakly bound molecular chemisorption state could give rise to the reaction observed by Cox and co-workers in their flow tube studies.[39] We searched for adduct formation down to a collision energy of 0.2 eV but did not observe any. This is not surprising because without collisional stabilization an adduct bound by only 0.35 eV would dissociate much too rapidly to be directly observed in our experiments. As discussed above, the $Al_{25}CO^+$ adduct we observe probably arises from dissociative chemisorption. Dissociative chemisorption of CO has been reported on alkali promoted aluminum surfaces.[44] It was found that with either potassium or sodium, CO dissociated after annealing to 700 K to yield aluminum oxide and aluminum carbide (cf. the $Al_{23}C^+ + Al_2O$ products we observe). It would clearly be fascinating to see if the activation barrier for dissociative chemisorption of CO on Al_{25}^+ could be lowered by a preadsorbed alkali atom.

We have already briefly discussed the interaction of oxygen with aluminum surfaces. Oxygen dissociatively chemisorbs on aluminum and then migrates to form an underlayer.[37] We found an activation barrier of 0.55 eV for the reaction between Al_{25}^+

(36) Ruatta, S. A.; Anderson, S. L. *J. Chem. Phys.*, submitted for publication.
(37) Batra, I. P.; Kleinman, L. *J. Electron Spectrosc. Relat. Phenom.* **1984**, *33*, 175.
(38) Saillard, J.-Y.; Hoffmann, R. *J. Am. Chem. Soc.* **1984**, *106*, 2006.
(39) Cox, D. M.; Trevor, D. J.; Whetten, R. L.; Kaldor, A. *J. Phys. Chem.* **1988**, *92*, 421.
(40) Parks, E. K.; Liu, K.; Richtsmeier, S. C.; Pobo, L. G.; Riley, S. J. *J. Chem. Phys.* **1985**, *82*, 5470.
(41) Paul, J.; Hoffmann, F. M. *Chem. Phys. Lett.* **1986**, *130*, 160.
(42) Bagus, P. S.; Bauschlicher, C. W.; Nelin, C. J.; Laskowski, B. C.; Seel, M. *J. Chem. Phys.* **1984**, *81*, 3594.
(43) Persson, B. N. J.; Muller, J. E. *Surf. Sci.* **1986**, *171*, 219.
(44) Paul, J.; Hoffmann, F. M. *J. Chem. Phys.* **1987**, *86*, 5188.

Table III. Summary of Activation Barriers Measured for Dissociative Chemisorption on Al_{25}^+

reaction	activation barrier, eV
$Al_{25}^+ + D_2$[a]	1.99
$Al_{25}^+ + CH_4$	3.47
$Al_{25}^+ + O_2$	0.55
$Al_{25}^+ + CO$	1.93
$Al_{25}^+ + N_2$	3.53

[a] From ref 17.

and O_2. This activation barrier is slightly larger than those found by Anderson and co-workers[35,36] for Al_2^+–Al_9^+ (although the error bars do overlap for some of the clusters). There is no significant activation barrier for chemisorption on aluminum surfaces[36] so the observation of an apparent overall increase in the activation barrier on going from Al_2^+ to Al_9^+ and then up to Al_{25}^+ is surprising. The origin of the increase in activation barrier with cluster size is not clear. It may be worth noting, however, that we found an increase in the activation barrier for chemisorption of D_2 from around 1 eV for Al_{10}^+ up to around 2 eV for Al_{27}^+.[17] These increases in the activation barriers with cluster size may reflect a significant change in the electronic properties of the clusters.

We have been unable to find very much information on the chemisorption of N_2 or CH_4 on aluminum surfaces. It seems unlikely that either N_2 or CH_4 dissociatively chemisorbs on aluminum at room temperature. Nitrogen apparently weakly physisorbs at low temperatures.[45] However, under severe conditions (1600 °C and 100 atm) nitrogen reacts with aluminum to yield aluminum nitride.[46]

(G) Comparison with Models for Bond Activation. Table III summarizes the information we have obtained so far on the activation barriers for dissociative chemisorption on Al_{25}^+. The result for D_2 is taken from our previous work.[17] This is the first time that activation barriers for dissociative chemisorption on a size selected cluster have been measured for a number of different molecules. One particularly noteworthy feature is the enormous range in the values for the activation barriers, from 0.55 eV up to 3.53 eV. Such a large range is difficult to cover in surface studies.

Obviously we would like to understand what determines the size of the activation barriers. As we have mentioned above, there is apparently no correlation with the strength of the bond being broken. However, it is reasonable to believe that the strength of the bonds that are formed could also be a factor. Shustorovitch[47] has used a simple analytical approach to this problem using Morse potentials. He derived the following expression for the activation barrier for dissociative chemisorption of a homonuclear diatomic A_2:

$$E_{act} = D(A_2) - kQ_A \quad (9)$$

where $D(A_2)$ is the dissociation energy of A_2, k is a constant with a value of 1.5, and Q_A is the binding energy of A to the surface. This simple model appears to have some success in accounting for the activation barriers found for the chemisorption of a number of simple molecules on transition metal surfaces.[47] Using some rather crude estimates of the binding energies (Q_A),[48] it appears that the predictions of this model (see Table IV) are in very rough qualitative agreement with the trends in our experimental measurements. So the strength of the bonds being broken and formed is probably a factor in determining the size of the activation barrier, but this is probably not the whole story.

Table IV. Activation Barriers Estimated from the Analytical Model of Shustorovitch[46]

molecule	activation barrier, eV[a]
D_2	~1
CH_4	~2
O_2	<0
CO	~1
N_2	~3

[a] Based on crude estimates of binding energies; see ref 47.

The Exxon group[37,49,50] have proposed an entirely different type of model in an attempt to rationalize their observations on the reactivity of neutral metal clusters studied using a fast flow reactor. Their model is based on frontier orbital arguments. At long range the interaction between a molecule such as hydrogen and a metal cluster is repulsive because the electrons are spin paired. At short range charge donation from the cluster to the H_2 σ^* orbital and from the H_2 σ orbital to the cluster weakens the H_2 bond and leads to an attractive bonding interaction. The strength of the interaction depends on the energy difference between the various orbitals. The size of the activation barrier is determined by interplay of the long-range repulsion and shorter range attractive forces. This model is based on solid concepts. The role of charge transfer has been noted in a number of recent theoretical studies on the chemisorption of hydrogen and other molecules on surfaces, clusters, and organometallic complexes.[38,47,51,52]

These arguments have been used to rationalize an apparent correlation between reactivity and cluster ionization potential.[49,50] For example, with Fe clusters[49] it was found that a low reactivity for chemisorbing hydrogen was correlated with a high cluster ionization potential, suggesting that charge transfer from the metal cluster to the H_2 σ^* orbital stabilized the transition state and reduced the activation barrier. These ideas are not universally accepted, however. Smalley and co-workers compared the reactivity of neutral clusters and cluster ions and found their reactivity patterns to be very similar.[53] Since positive ions have much less tendency to donate charge, it was argued that the factor controlling the cluster reactivity was, in fact, cluster structure (the ions and neutrals are expected to have roughly the same structures). More recently Upton[52] has reported theoretical calculations on the dissociative chemisorption of H_2 on Al_6, Al_6^+, and Al_6^-. He found that the activation barrier and the degree of donation to the H_2 σ^* orbital was not strongly affected by the presence of the charge. He rationalized this result by pointing out that a dipole interaction results from charge transfer which is stabilizing for the cation and destabilizing for the anion. At least in the case of Al_6 it appears that this dipole interaction largely cancels the effect of the ionization potential differences.

Adapting the ideas discussed above, we might expect to find a low activation barrier for a molecule with a low-lying antibonding orbital since charge donation from the cluster will lower the transition-state energy. Similarly, a low activation barrier would be expected for a molecule with a high-lying occupied molecular orbital. A similar approach has recently been used by Cox and co-workers.[39] In Figure 11 we have plotted the energies of the highest occupied molecular orbital (HOMO) and lowest unfilled molecular orbital (LUMO) of the molecules studied.[54] The

(45) Mayer, O.; Fromm, E. *Z. Metallkd.* **1977**, *68*, 27.
(46) Wade, K.; Banister, A. J. In *Comprehensive Inorganic Chemistry*; Bailar, J. C., Emeleus, H. J., Nyholm, R., Trotman-Dickenson, A. F., Eds.; Pergamon: Oxford, 1971; Vol. 1, p 1038.
(47) Shustorovitch, V. *Surf. Sci. Rep.* **1986**, *6*, 1.
(48) The estimates of the binding energies for H and O to the cluster are discussed in ref 17 and 19. The estimates for the other species were obtained using the approach in ref 17. The estimates for H and O are the most reliable.
(49) Whetten, R. L.; Cox, D. M.; Trevor, D. J.; Kaldor, A. *Phys. Rev. Lett.* **1985**, *54*, 1494.
(50) Trevor, D. J.; Kaldor, A. *ACS Symp. Ser.* **1987**, *No. 333*, 43.
(51) See, for example: Hjelmberg, H. *Surf. Sci.* **1979**, *81*, 539. Upton, T. H. *J. Am. Chem. Soc.* **1984**, *106*, 1561. Partridge, H.; Bauschlicher, C. W. *J. Chem. Phys.* **1986**, *84*, 6507. Baetzold, R. C. *J. Am. Chem. Soc.* **1983**, *105*, 4271.
(52) Upton, T. H.; Cox, D. M.; Kaldor, A. In *Physics and Chemistry of Small Clusters*; Jena, P., Rao, B. K., Khanna, S. N., Eds.; Plenum: New York, 1987; p 755.
(53) Alford, J. M.; Weiss, F. D.; Laaksonen, R. T.; Smalley, R. E. *J. Phys. Chem.* **1986**, *90*, 4480. Brucat, P. J.; Pettiette, C. L.; Yang, S.; Zheng, L.-S.; Craycraft, M. J.; Smalley, R. E. *J. Chem. Phys.* **1986**, *85*, 4747.
(54) Orbital energies taken from: Jorgensen, W. L.; Salem, L. *The Organic Chemist's Book of Orbitals*; Academic: New York, 1973.

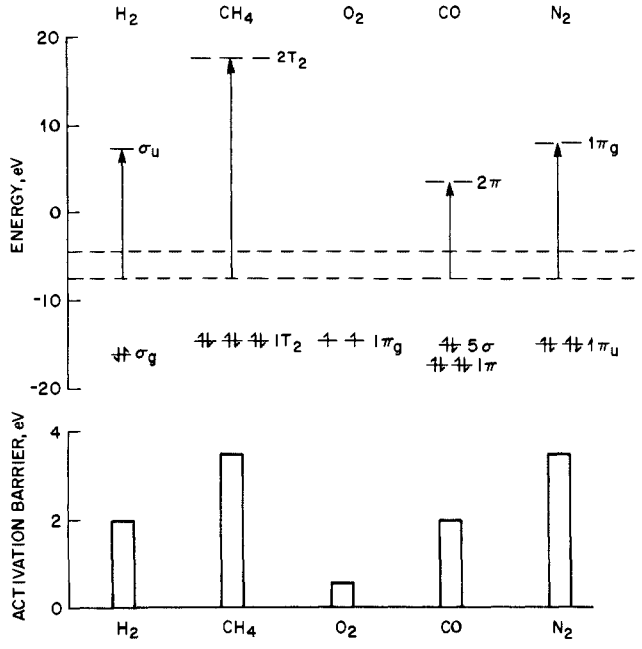

Figure 11. Diagram showing the energies of the highest occupied molecular orbital and lowest unfilled molecular orbital of the molecules studied. The orbital energies were taken from ref 53. The dashed lines show the first and second ionization potential of Al_{25} (see text) and the arrows give the promotion energies. The lower half of the diagram shows the measured activation barriers.

dashed lines show the first and second ionization potentials of Al_{25}. While reasonably reliable values for the first ionization potential of Al_{25} are available,[20,39] there have been no experimental determinations of the second ionization potential. Brechignac and co-workers[55] have recently reported appearance potentials for doubly charged mercury clusters, Hg_n^{2+}; for $n = 5$–15 the second ionization potential is approximately 3 eV larger than the first. The difference could be smaller for Al_{25} because it ultimately vanishes with increasing cluster size. However, we have used this value in Figure 11.

It is apparent from Figure 11 that the HOMOs of the molecules studied have roughly the same energy. However, the LUMO energies are dramatically different. So we will focus on charge donation from the metal cluster to the antibonding orbitals. This is reasonable because it has been suggested that the interaction with the antibonding orbitals is stronger since they extend further giving rise to better overlap.[38,47] It is clear that there is a rough correlation between the promotion energies from the cluster to the lowest unfilled molecular orbitals (shown as the arrows in Figure 11) and the measured activation barriers, but we need to be careful about interpreting these results because the orbitals involved are different and other factors could also be important.

In the case of H_2 and CH_4 we are dealing with σ and σ^* orbitals, and the increase in activation barrier on going from H_2 to CH_4 could be partly due to a significantly higher energy σ^* orbital in CH_4. We have already mentioned above that steric factors could also contribute to the higher activation barrier observed for CH_4. A geometry with the C–H bond aligned with the metal is favored over the perpendicular configuration.[38]

The oxygen molecule has a triplet ground state with its highest occupied molecular orbital unfilled, so with the above model we would expect no activation barrier. The reaction with oxygen does show the lowest activation barrier of the molecules studied. However, we would also expect no activation barrier from the analytical model of Shustorovitch[47] because of the extremely strong Al–O bonds formed.

With CO and N_2 the situation is slightly different. We are dealing with π orbitals. Charge transfer will not be so effective in weakening the stronger CO and N_2 bonds, and can lead to molecular chemisorption. For example, molecular chemisorption of CO on metal surfaces is believed to involve charge donation from the CO 5σ orbital (which is largely nonbonding) to the metal, and back-donation from the metal to the $2\pi^*$ orbitals on CO.[56] As can be seen from Figure 11, the energy of the $1\pi_g$ orbital of N_2 is substantially higher in energy than the $2\pi^*$ orbital of CO. This suggests that charge transfer to the antibonding orbitals could play a role in stabilizing the transition state and account for the larger activation barrier observed for N_2 chemisorption on Al_{25}^+. Theoretical calculations[42,43] indicate that molecular chemisorption of CO on aluminum is mainly due to donation to the CO $2\pi^*$ orbitals. It is not unreasonable to expect the same interaction to stabilize the transition state for dissociative chemisorption.

We have not yet considered how the electronic structure of the metal cluster could play a role. That the electronic structure of the metal is important can easily be seen from recent studies of the chemisorption of H_2 on Fe and Cu clusters in a flow reactor.[49,57] The Fe clusters react and the reactivity shows a rough correlation to the cluster ionization potential. The Cu clusters do not react although some have ionization potentials as low as the reactive Fe clusters. These results suggest that electronic structure of the metal cluster (in this case the presence of an unfilled d shell) will also have an important effect on the activation barriers.

For hydrogen chemisorption on aluminum clusters we found that activation barriers increased from a little over 1 eV to around 2 eV for clusters with 10–27 atoms.[27] The ionization potentials of the aluminum clusters drop with increasing cluster size so the trends in the activation barriers for hydrogen chemisorption are the reverse of what would be expected from the charge transfer model for bond activation. On the other hand, the correlation between the activation barriers for Al_{25}^+ and the LUMO promotion energies shown in Figure 11 suggest that donation of electron density to the antibonding orbitals is an important factor in determining the size of the activation barrier. To resolve this conflict we suggest that while charge transfer may be an important factor in determining the size of the activation barriers, other electronic factors (which change with cluster size) are also important. These other factors account for the increase in activation barrier with cluster size observed for D_2 chemisorption. Without detailed calculations it is difficult to speculate what these other electronic factors may be. One possibility, for example, is the overlap of the 3s and 3p bands which will increase the free electron density. Jellium model calculations[58] for hydrogen chemisorption on bulk Na, Mg, and Al suggest that the activation barrier is due to a repulsive interaction between the hydrogen molecule and the electron density which spills over the jellium edge. The activation barriers increase along the series Na, Mg, and Al as the free electron density increases.

Summary and Conclusions

In this paper we have presented a detailed study of the reactions between CO, N_2, O_2, and CH_4 with size selected Al_{25}^+ clusters. For CO, N_2, and CH_4 an adduct arising from chemisorption onto the cluster was directly observed. In all cases it appeared that dissociative (rather than molecular) chemisorption was occurring. Activation barriers for chemisorption were deduced from simulations of the cross sections for adduct formation. With O_2 no adduct was observed, presumably because a highly exothermic reaction follows dissociative chemisorption. However, an activation barrier was deduced from the reaction cross sections. It appears that the activation barrier for Al_{25}^+ with O_2 is slightly larger than those measured by Anderson and co-workers for Al_2^+–Al_9^+.[35,36] The activation barrier must presumably approach the bulk value for clusters larger than Al_{25}^+. The activation barriers obtained from this work and from our previous work with D_2[17] were compared with the predictions of simple models. The size of the activation barriers appear qualitatively consistent with the charge

(55) Brechignac, C.; Broyer, M.; Cahuzac, Ph.; Delacretaz, G.; Labastie, P.; Woste, L. *Chem. Phys. Lett.* **1985**, *118*, 174.

(56) Engel, T.; Ertl, G. *Adv. Catal.* **1979**, *28*, 1.

(57) Morse, M. D.; Geusic, M. E.; Heath, J. R.; Smalley, R. E. *J. Chem. Phys.* **1985**, *83*, 2293.

(58) Johansson, P. K. *Surf. Sci.* **1981**, *104*, 510.

transfer model for bond activation. However, it was pointed out that other factors probably also play a major role in determining the size of the activation barriers.

Finally, we would like to point out that the data presented here provide an excellent opportunity for comparison with theoretical calculations. The results are for a simple sp metal, and the dramatic differences observed in the activation barriers for different molecules lead us to believe that the important factors in these reactions could be deduced from quite modest calculations. In contrast, attempts to perform theoretical calculations on, for example, Fe clusters with the precision required to explain why Fe_{18} reacts slower by a factor of 1000 than Fe_{25}[1] are not likely to be very enlightening because the activation barriers only differ by at most 0.2 eV.

Metal Ion Substitution Chemistry in the YBaCuO System as a Probe of the Superexchange Pathway

Ruth Jones,[1a] Peter P. Edwards,*[,1a] Martin R. Harrison,[1b] Thitinant Thanyasiri,[1c] and Ekkehard Sinn*[,1c]

Contribution from University Chemical Laboratory, Lensfield Road, and Interdepartmental Research Center for Superconductivity, Cambridge University, Cambridge CB2 1EW, Great Britain, GEC Research, Hirst Research Centre, Wembley, Great Britain, and Chemistry Department, University of Virginia, Charlottesville, Virginia 22901.
Received September 15, 1987

Abstract: The effect of substitution for Cu by aluminum, nickel, and zinc in the YBaCuO superconducting system is described in detail. All three metals lower the T_c value and make the superconducting transition less abrupt. However, the strength of the effect varies with the metal, and this is attributed to their different reactivities and site preferences. The most dramatic effect is with zinc, which completely quenches the superconductivity when as few as 10% of the Cu sites are replaced. It is postulated that under these synthetic conditions zinc prefers the five-coordinated "Cu(2)" site, which is presumed to lie on the main superconducting pathway. Nickel has a stronger affinity for the four-coordinated "Cu(1)" sites and is apparently found in both sites at high dopant levels. Magic angle spinning NMR (MAS NMR) and other data indicate that Al prefers the four-coordinate Cu(1) site for initial substitution, although aluminum ions may also aggregate at the twinning boundaries. We suggest the hypothesis that substitution of the Cu(1) sites eliminates their contribution to the superconductivity and thereby makes the system like the related 40 K superconductors, which lack the Cu(1) sites.

Superconductivity was initially discovered in pure metals,[2] but higher transition temperatures, up to $T_c = 23$ K, were observed in alloys, especially with niobium.[3] Searches for new superconductors tended to center on the immediate neighborhood of Nb in the periodic table. The known inorganic superconductors[4] received more limited attention prior to the observation of $T_c = 36$–50 K in one series of copper oxide perovskites and $T_c > 90$ K in another.[5-8] We report substitution studies in the 90 K system, $YBa_2Cu_3O_{7-\delta}$, with the overall aim of elucidating the nature and mechanism of the superconducting path. This substitution chemistry is also crucially important in understanding and controlling the strong superconductor/substrate interaction during the preparation of thin-films materials. Here, the chemical reaction not only destroys the superconductivity of the deposited film but also dopes it with potentially detrimental impurities, which can degrade the superconducting properties and increase the normal-state resistivity.

Table I. O Content, $7 - \delta$, in $YBa_2Cu_{3-x}M_xO_{7-\delta}$

pure 123 phase	7% Zn	7% Ni	7% Al
6.89 (6.88[a])	6.99	6.92	6.79
6.89 (6.87[a])	6.91	6.89	6.83
	6.88	6.90	6.77

[a] TGA data on same sample.

The $YBa_2Cu_3O_{7-\delta}$ system possesses two crystallographically distinct and chemically dissimilar copper sites[9-11] (Figure 1): the square-planar Cu(1) chains and the square-pyramidal Cu(2) layers, separated by the large Ba^{2+} ions. Local charge neutrality considerations and a greater crystal field stabilization would favor the location of Cu^{3+} in the Cu(1) sites, and this would be balanced by a predominant but not exclusive Cu^{2+} occupancy of the Cu(2) sites. The Cu(2) sites are possessed by both the 40 and 90 K

(1) (a) Cambridge University. (b) GEC Research. (c) University of Virginia.
(2) Kammerlingh-Onnes, H. *Leiden Commun.* **1911**, 122b, 124c.
(3) Testardi, L. R.; Meek, R. L.; Poate, J. M.; Royer, W. A.; Storm, A. R.; Wernick, J. H. *Phys. Rev. B: Solid State* **1975**, *B11*, 4304.
(4) Chevrel, M.; Sergent, J.; Prigent, J. *J. Solid. State Chem.* **1971**, *3*, 515. Johnson, D. C.; Prakash, H.; Zachariasen, W. H.; Viswanathan, R. *Mater. Res. Bull.* **1973**, *8*, 777. Sleight, A. W.; Gillson, J. L.; Bierstedt, P. E. *Solid State Commun.* **1975**, *17*, 299.
(5) Bednorz, J. G.; Muller, K. A. *Z. Phys. B: Condens. Matter* **1986**, *64*, 189.
(6) Wu, M. K.; Ashburn, J. R.; Torng, C. J.; Hor, P. H.; Meng, R. L.; Gao, L.; Huang, Z. J.; Wang, Y. Q.; Chu, C. W. *Phys. Rev. Lett.* **1987**, *58*, 908.
(7) Jones, R.; Ashby, M. F.; Campbell, A. M.; Edwards, P. P.; Harrison, M. R.; Hibbs, A. D.; Jefferson, D. A.; Kirkland, A. I.; Thanyasiri, T.; Sinn, E. *ACS Symp. Ser.* **1987**, *351*.
(8) Nelson, D. L., Whittingham, M. S., George, T. F., Eds. Proceedings of Symposium by the Inorganic and Physical Chemistry Divisions of the American Chemical Society, presented at the 194th National Meeting of the American Chemical Society, New Orleans, LA, Aug-Sept 1987.
(9) David, W. I. F.; Harrison, W. T. A.; Gunn, J. M. F; Moze, O.; Soper, A. K.; Day, P.; Jorgenson, J. D. Hinks, B. G.; Beno, M. A.; Soderholm, L.; Capone, D. W., II; Schuller, I. K.; Segre, C. U.; Zhang, K.; Grace, J. D. *Nature (London)* **1987**, *327*, 310.
(10) Steinfink, H.; Swinnea, J. S.; Sui, Z. T.; Hsu, H. M.; Goodenough, J. B. *J. Am. Chem. Soc.* **1987**, *109*, 3348.
(11) Murphy, D. W.; Sunshine, S.; van Dover, R. B.; Cava, R. J.; Batlogg, B.; Zahurak, S. M.; Schneemeyer, L. F. *Phys. Rev. Lett.* **1987**, *58*, 1888.

0002-7863/88/1510-6716$01.50/0